Journal of Materials Processing Tech. 267 (2019) 52–60

Contents lists available at ScienceDirect

Journal of Materials Processing Tech.

journal homepage: www.elsevier.com/locate/jmatprotec

Enhancing strength without compromising ductility in copper by combining extrusion machining and heat treatment

Yao Liu[a], Songlin Cai[b,*], Fengguang Xu[c], Yunjiang Wang[d,e], Lanhong Dai[d,e,**]

[a] School of Mathematics and Physics, University of Science and Technology Beijing, Beijing 100083, PR China
[b] China Electric Power Research Institute, State Grid Corporation of China, Beijing 100192, PR China
[c] Basic Experimental Center for Natural Science, University of Science and Technology Beijing, Beijing 100083, PR China
[d] State Key Laboratory of Nonlinear Mechanics, Institute of Mechanics, Chinese Academy of Sciences, Beijing 100190, PR China
[e] School of Engineering Science, University of Chinese Academy of Sciences, Beijing 101408, PR China

ARTICLE INFO

Associate editor: Z. Cui

Keywords:
Extrusion machining
Heat treatment
Mechanical property
Recrystallization
Subgrains

ABSTRACT

It is a challenge to produce metallic materials with high strength and good ductility. Improving the strength of metallic materials usually sacrifices the ductility or work-hardening capacity. Here combining extrusion machining and heat treatment, we improve the strength of copper without losing strain hardening capacity and therefore the ductility remains. Copper was first deformed by extrusion machining at shear strain 3.1 and then annealed at 523 K for 5 min. Compared with the initial workpiece, the processed copper possesses five times higher yield strength and alike work hardening behavior. Microstructural characterizations illustrate that high strength and high strain hardening are attributed to the hierarchical microstructure that the recrystallized grains are surrounded by elongated subgrains. Finally, an analytical modeling was employed to rationalize the mechanical properties of copper processed by the proposed strategy. The theoretical results are in agreement with the experimental measurements.

1. Introduction

High strength and high ductility are demanded for the application of engineering materials. Strength can be improved by the well-known methods such as grain refinement (Güzel et al., 2012), solid solution alloying (Su et al., 2008), work hardening (Lobos et al., 2010), and introducing strengthening phases (Dolata-Grosz et al., 2006). As demonstrated by Valiev et al. (2000), strength and ductility are contradictory in metallic materials. According to Meyers et al. (2006), improving the strength of materials usually leads to poor ductility or work-hardening capacity. Jia et al. (2001) found that the poor ductility always stemmed from the low strain hardening in materials. Zhu and Liao (2004) further found that high strain hardening rate helped to restrain localized deformation and postpone necking. Wu et al. (2014) reported that high-strength metals would need a higher strain hardening rate to maintain the ductility.

Specific microstructures could be designed to improve the strain hardening rate in high-strength metals. Wang et al. (2002) proposed a bimodal grain size distribution to induce strain hardening mechanisms in high-strength copper. Lu et al. (2004) noted that nano-twinned copper possessed extra-high strength with keeping the ductility within a certain regime. Petryk et al. (2008) investigated the effect of dislocation cell and cell-block boundaries on grain refinement and strain hardening in interstitial free steel. Fang et al. (2011) reported that gradient nano-grained structures above coarse grained copper contributed to both strength and ductility. Kauffmann et al. (2013) presented that the formation of non-coherent twin boundaries could result in an increase of strength but a loss of ductility in cryogenic drawn copper. Liu et al. (2016a) used topologically controlled surface mechanical attrition treatment (SMAT) to produce planar heterogeneous structure in copper with high strength but no sacrifice of ductility. Huo et al. (2017) employed a simplified thermo-mechanical treatment to prepare fine-grained Al-Zn-Mg-Cu alloy with notably improved ductility and maintained high strength. Tian et al. (2018) stated that the recrystallized ultrafine-grained copper with a minimum mean grain size of 0.51 μm showed high strength and good ductility.

As proved by Childs (2013), machining is an effective strategy to impose severe plastic deformation (SPD) in metallic materials. Compared with the conventional SPD methods, e.g. equal channel angular pressing (ECAP) (Segal et al., 1981), high-pressure torsion (HPT)

* Corresponding author.
** Corresponding author at: State Key Laboratory of Nonlinear Mechanics, Institute of Mechanics, Chinese Academy of Sciences, Beijing 100190, PR China.
E-mail addresses: caisonglin@lnm.imech.ac.cn (S. Cai), lhdai@lnm.imech.ac.cn (L. Dai).

https://doi.org/10.1016/j.jmatprotec.2018.12.001
Received 15 June 2018; Received in revised form 14 October 2018; Accepted 1 December 2018
Available online 03 December 2018
0924-0136/

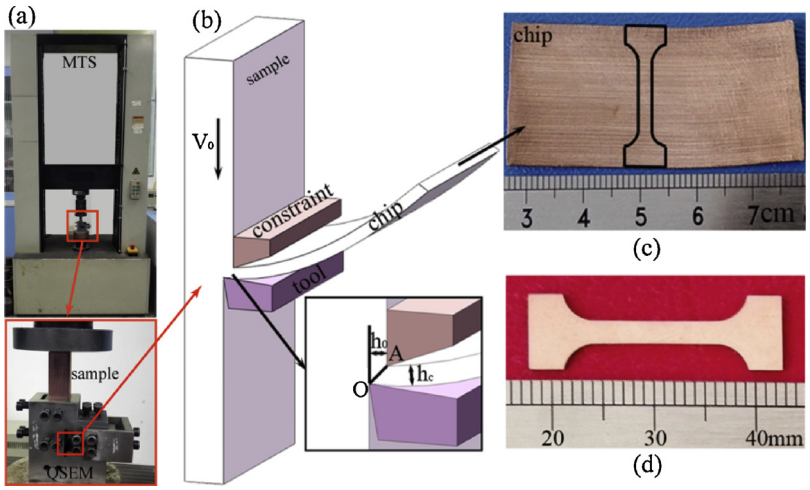

Fig. 1. (a) Experimental equipment for quasi-static extrusion machining (QSEM). (b) Schematic of QSEM magnification. (c) Copper sheet after QSEM and the sampling method of tensile specimen. (d) Sample for uniaxial tensile tests.

Table 1
Machining parameters in quasi-static extrusion machining (QSEM).

Machining parameters	Notation	Value
Rake angle	α	10°
Precut chip thickness	h_0	200 μm
Cutting speed	V_0	2 mm/min
Controlled chip thickness	h_c	600, 500, 300 μm
Shear strain in primary shear zone	γ	3.1, 2.8, 2.5

(Smirnova et al., 1986), accumulative roll binding (ARB) (Saito et al., 1999) and cyclic extrusion compression (CEC) (Richert et al., 1999), machining needs only a single pass of room-temperature deformation process to achieve SPD. Ceretti et al. (1999) and Umbrello et al. (2008) conducted numerical simulation of machining to investigate the influence of machining parameters on large deformation filed. Moscoso et al. (2007) employed the SPD method of extrusion machining to produce bulk nanostructured copper. Brown et al. (2009) further investigated the effects of extrusion machining parameters (strain, strain rate and temperature) on the microstructural evolution and Vickers hardness. By means of high speed extrusion machining, Liu et al. (2016b) fabricated a bimodal grain size distributed magnesium alloy with high Vickers hardness.

Machining, as a method of SPD, has been used to process materials with specific microstructure and high Vickers hardness. However, it is unknown whether extrusion machining could fabricate materials with high strength and good ductility. In this paper, extrusion machining and heat treatment were combined to research the relationship between machining parameters and mechanical properties. Uniaxial tensile tests and microstructural characterizations were further performed to investigate the effect of controlled microstructure on strength and strain hardening. Finally, a theoretical model was employed to reveal the mechanism underlying the proposed strategy.

2. Experimental procedure

Oxygen-free-high-conductivity (OFHC) copper with the purity of 99.95% was used here. A copper cuboid with dimensions of $25 \times 25 \times 80$ mm^3 was annealed in vacuum at 773 K for 1 h to obtain homogeneous coarse grain (CG) microstructure. The copper samples were processed by means of quasi-static extrusion machining (QSEM) at the room temperature (Fig. 1a). The tool with a precut thickness h_0 is cutting the workpiece at the cutting speed V_0 (Fig. 1b). The chip thickness h_c is controlled by the constraint. The different chip thicknesses in Table 1 were obtained by adjusting the relative position between tool and constraint. The wedge-shaped tool with a rake angle α is machining the workpiece and then the materials flow out along the rake face in the form of a chip due to a process of shear in primary shear zone (PSZ). Based on shear strain formula from Cai et al. (2015), shear strains γ in PSZ are illustrated in Table 1. QSEM was conducted under the conditions in Table 1 and then chips were collected to be bulk copper sheets (Fig. 1c). After QSEM, the bulk copper sheets were

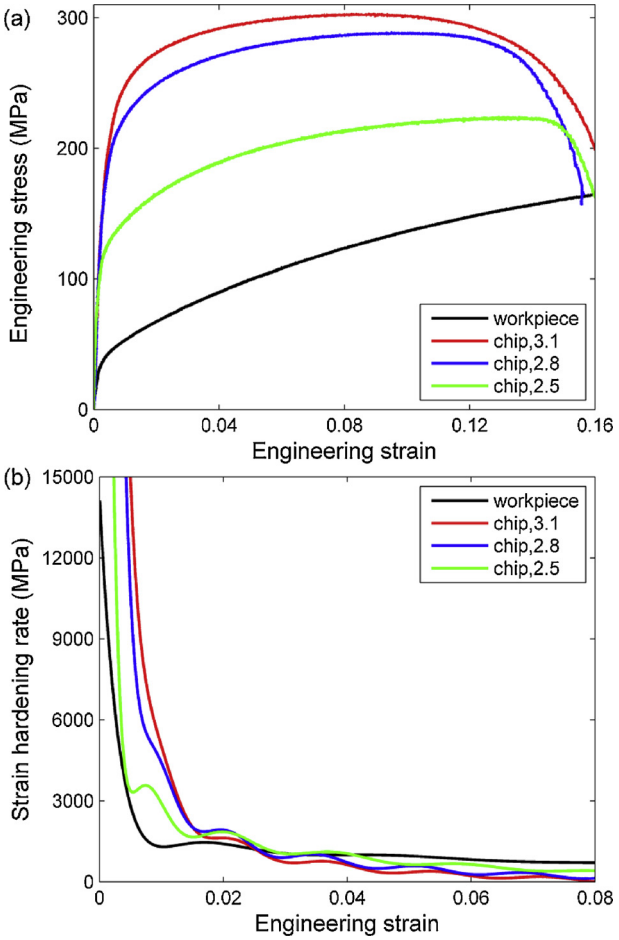

Fig. 2. (a) Engineering stress-strain curves of different shear strain processed copper. (b) Strain hardening rate versus engineering strain for different shear strain processed copper.

Table 2
Tensile test results of the initial workpiece and the processed copper sheets with different shear strains.

Controlled chip thickness	Shear strain	0.2% yield strength	Strain hardening rate
Initial workpiece	0	47 ± 2 MPa	1064 ± 95 MPa
600 μm	3.1	245 ± 10 MPa	811 ± 74 MPa
500 μm	2.8	218 ± 9 MPa	945 ± 86 MPa
300 μm	2.5	135 ± 11 MPa	1059 ± 102 MPa

annealed at 523 K for 5 min. The partial recrystallization could happen in bulk copper sheets during heat treatment (HT). After HT, specimens for uniaxial tensile tests were cut from bulk copper sheets (see Fig. 1c-d).

All tensile specimens were prepared with a gauge length of 12 mm and a width of 2.5 mm. All tensile tests were repeated at least 3 times. Quasi-static uniaxial tensile tests were carried out on Instron E10000 with a strain rate of 2.5×10^{-4} s^{-1} at room temperature. Electron backscatter diffraction (EBSD) was performed to investigate the microstructural evolution using JOEL JSM-7800 F at the operating voltage of 15 kV. The specimens for EBSD were prepared by polishing with SiC (down to 2000 grit) and further vibratory polishing for 8 h. The scanning step length was 5 μm and 0.5 μm for initial workpiece and processed samples respectively. According to ASTM E112-10 method proposed by Jiang et al. (2014) and Nag et al. (2014), the average grain sizes can be measured by the morphologies procedure in the image analysis software (Image Pro-Plus 6.0). Transmission electron microscope (TEM) observation was carried out on JEM 2010 with the operating voltage of 200 kV. The samples for TEM were polished down to about 70 μm and then the solution of 20 ml phosphoric acid, 20 ml alcohol and 80 ml water was used for double jet at 273 K to get thin area.

X-ray diffraction (XRD) was used to study the evolution of dislocation density. The XRD measurements of copper sheets were carried out on a Bruker D8 Focus X-ray diffractometer. A rotating Cu target was used with a voltage of 40 kV and a current of 40 mA. The X-ray wavelength $\lambda_{K\alpha 1}$ is 1.54056 Å. The specimens for XRD measurements were mechanically ground and finally electropolished to minimize the possible error. The diffraction lines were recorded from 40°to 101°with a step of 0.02°to cover the diffractions of (111), (200), (220), (311) and (222). Data analyses were performed by using the MDI Jade 6.5 software. The instrumental broadening profiles were obtained by XRD of the SiO_2 reference sample. The experimental Bragg reflections were fitted by the Pseudo-Voigt function (a linear combination of the Lorentzian and Gaussian functions) (Cox et al., 1986), indicating that the instrumental broadening effect is removed from the measured intensity profile. The physical profile of processed copper is caused by the small size of the diffracting grains and the lattice strain broadening.

3. Experimental results

3.1. Mechanical property

Fig. 2 shows the tensile behaviors of copper sheets as well as the initial workpiece for comparison. The engineering stress-strain curves were plotted in Fig. 2a. For the initial workpiece, the initial workpiece has the 0.2% yield strength of about 47 MPa. After QSEM and HT, the strength of copper was improved significantly (Fig. 2a). As shown in Table 2, the 0.2% yield strength increases with the increasing shear

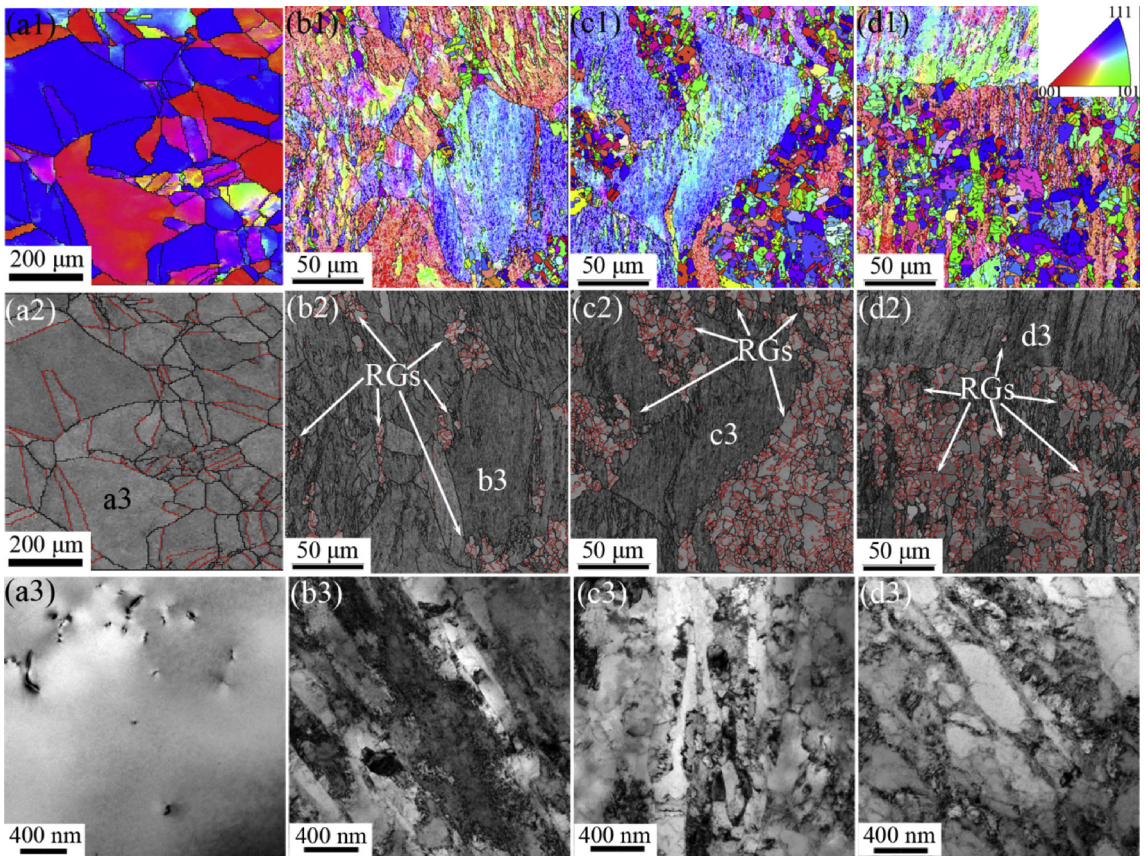

Fig. 3. (a1)-(d1) EBSD images in copper samples: (a1) initial workpiece; (b1) shear strain of 3.1; (c1) shear strain of 2.8; (d1) shear strain of 2.5. (a2)-(d2) are EBSD image quality map of (a1)-(d1) respectively: twin boundary labeled in red, high angle grain boundary labeled in black and recrystallized grains (RGs) illustrated by arrows. (a3)-(d3) are TEM micrographs in the testing positions illustrated in (a2)-(d2) respectively (For interpretation of the references to colour in this figure legend, the reader is referred to the web version of this article).

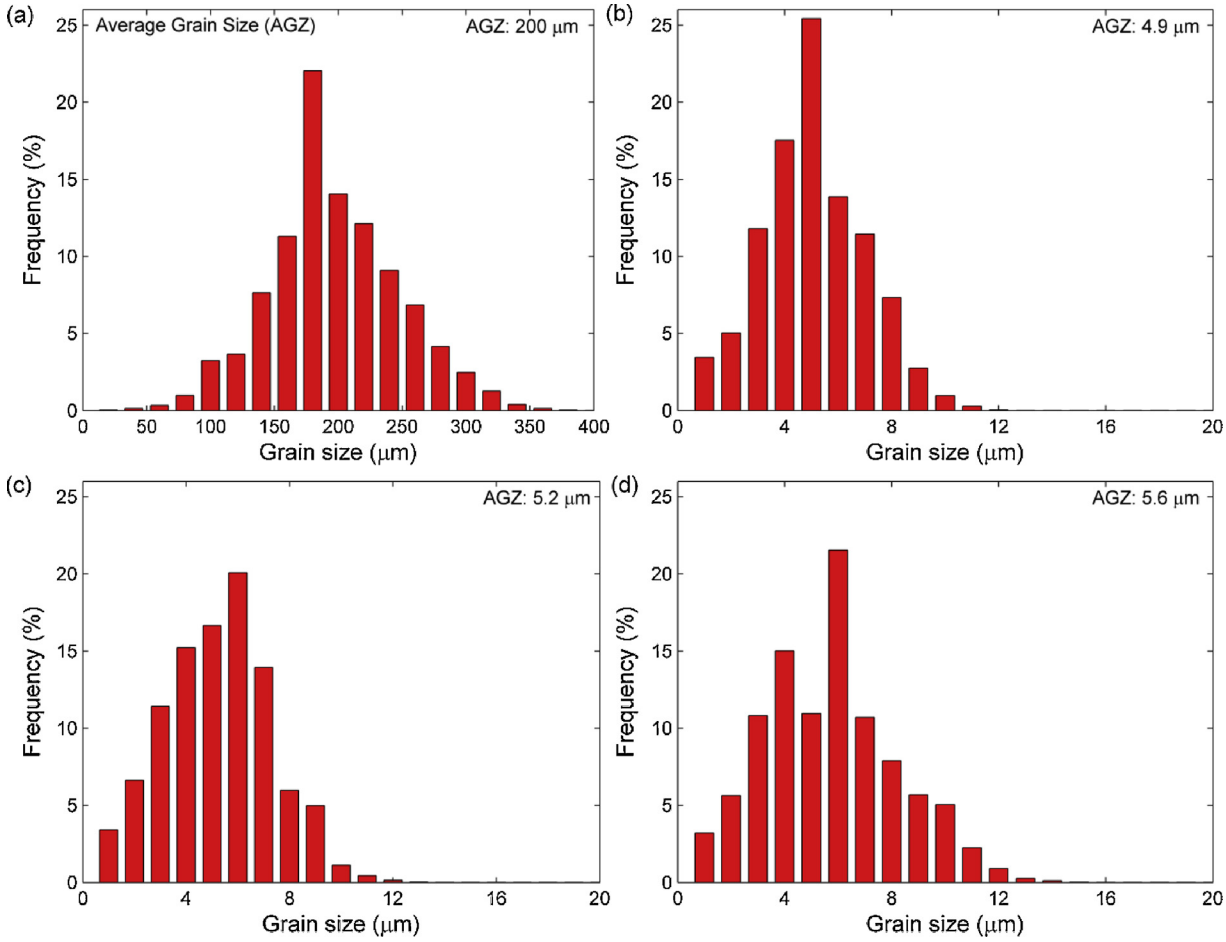

Fig. 4. Grain size distribution: (a) initial workpiece; (b)-(d) shear strains are 3.1, 2.8 and 2.5 respectively.

strain. The yield strength of copper sheet is ~245 MPa for the shear strain of 3.1, which is five times higher than that of the initial workpiece. Fig. 2b shows the strain hardening rate versus engineering strain curve. At the beginning of tensile deformation ($\varepsilon < 0.02$), the strain hardening rate of copper sheet is higher than that of the initial workpiece. The strain hardening rate of copper sheet increases with the increasing shear strain. However, there is no distinct difference for strain hardening rate when tensile strain exceeds 0.02 (Fig. 2b and Table 2). Copper sheets processed by QSEM and HT have enhanced strength but no significant reduction in strain hardening rate.

3.2. Microstructural characterization

Figs. 3 and 4 show microstructural characterization and grain size distribution respectively. The average grain size of initial workpiece is about 200 μm (Fig. 4a) and there are annealed twins in coarse grains (Fig. 3a2). As shown in Fig. 3a3, less dislocation appeared within CG in initial workpiece. After QSEM and subsequent HT, small recrystallized grains appeared in copper sheet (Fig. 3b1-d1) and annealed twins emerged in small recrystallized grains (Fig. 3b2-d2). Based on the grain size distribution in Fig. 4b-d, the average grain size of the small recrystallized grains is ~5 μm. Compared with the SPDed grains, the small recrystallized grains have less dislocation inside. The appearance of small recrystallized grains contributes to the improvement of strain hardening (Fig. 2). As shown in Fig. 3b2-d2, the volume fraction of recrystallized grains increases with the decreasing shear strain. According to TEM micrographs in Fig. 3b3-d3, the remained coarse grains contain elongated subgrains. The elongated subgrains have broad and diffuse low angle grain boundaries (LAGBs) consisting of forest dislocations. As demonstrated by Hall (1951) and Petch (1953), the elongated substructures with small misorientations and the small recrystallized grains help to enhance the strength of copper.

The microstructural characterization helps to reveal the mechanism of the similar strain hardening rate in Fig. 2b. When tensile strain exceeds 0.02, plastic deformation happens in both the initial workpiece and the processed copper (Fig. 2a). The processed copper contains SPDed grains and recrystallized grains. Because the SPDed grains are saturated with a great deal of forest dislocation during QSEM, they have no capacity to store new dislocation during tensile deformation. Compared with the SPDed grains, the recrystallized grains have less dislocation. Therefore, the dislocation should be stored in the recrystallized grains during tensile deformation. Both the initial workpiece and the processed coppers have recrystallized grains inside; therefore, they have alike dislocation storage capacity. This leads to the no distinct difference for strain hardening rate when tensile strain exceeds 0.02.

3.3. Misorientation angle distribution

The misorientation angle distributions of different copper samples are illustrated in Fig. 5. For initial workpiece, the frequency of misorientation angle below 5°is less than that of large misorientation angle (Fig. 5a). There are less LAGBs in the initial workpiece. The higher frequency of misorientation angle near 60°is observed in Fig. 5a, which indicates that the $\sum 3$ twin boundaries form in the initial workpiece. The $\sum 3$ twin boundaries were labeled in red in Fig. 3a2.

After QSEM and subsequent HT, the frequency of misorientation angle below 5°is more than that of large misorientation angle (Fig. 5b-

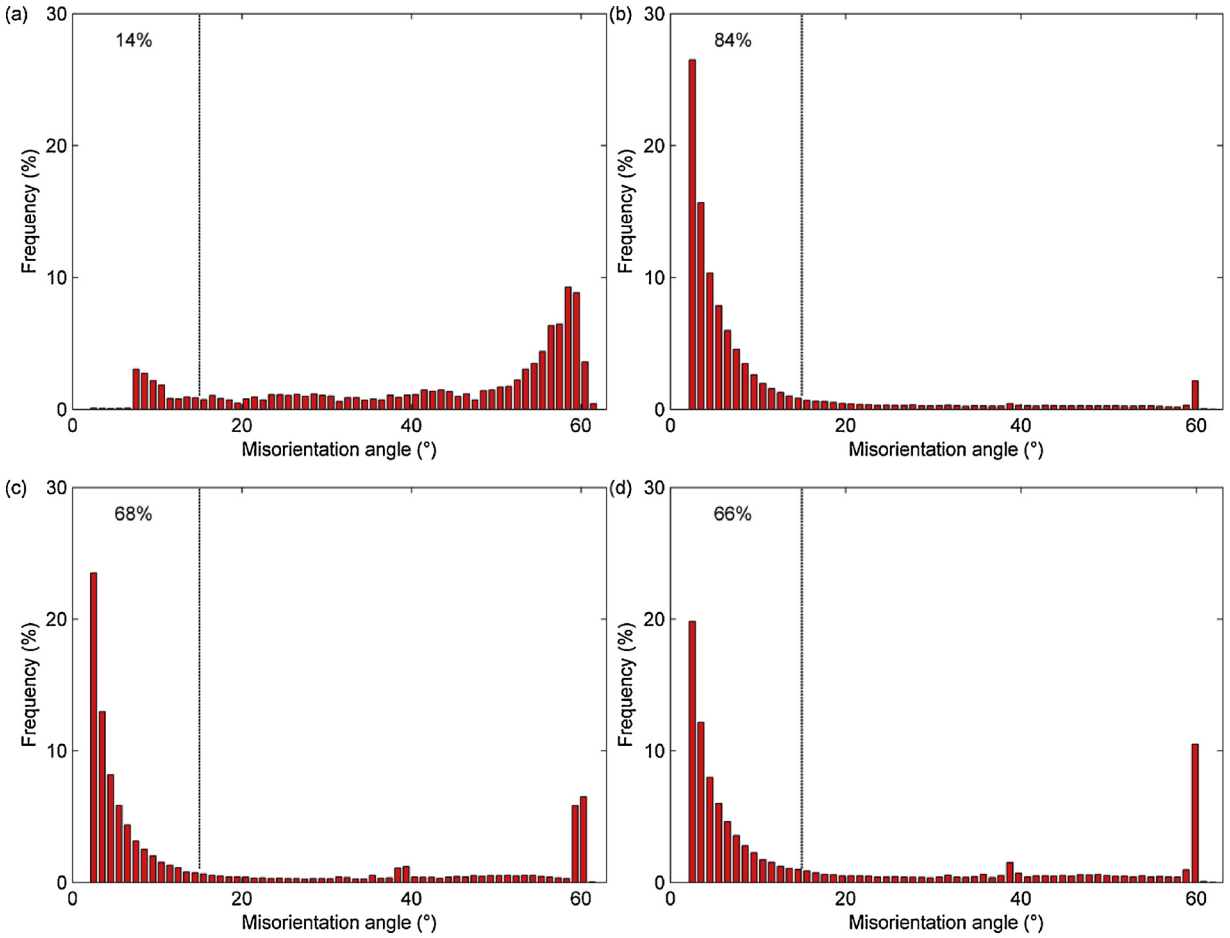

Fig. 5. Misorientation angle distribution in copper samples: (a) initial workpiece; (b)-(d) shear strains are 3.1, 2.8 and 2.5 respectively.

d). The increase of LAGBs indicates the formation of subgrains; therefore, elongated subgrains were observed in TEM micrographs (Fig. 3b3-d3). The accumulation of misorientation angle near 60°is attributed to the formation of $\sum 3$ twin boundaries in the recrystallized grains, which were labeled in red in Fig. 3b2-d2. From Fig. 5b-d, the frequency of misorientation angle below 5°decreases with the decreasing shear strain. The frequency of misorientation angle near 60°increases with the decreasing shear strain. The increase of LAGBs indicates the increase of forest dislocation and helps to strengthen the materials. Christian and Mahajan (1995) found that $\sum 3$ twin boundaries had coherent interfaces. Like conventional GBs, coherent $\sum 3$ twin boundaries can obstruct the motion of dislocations, which improves the strength of copper. Coherent $\sum 3$ twin boundaries can also provide a possible slip transfer, which increases the ability of accommodating more dislocation and possibly contributes to ductility (Lu et al., 2009).

3.4. Dislocation density evolution

Fig. 6a shows the typical XRD patterns of copper samples subjected to different shear strains. The reflection peaks are significantly broadened with the increasing shear strain, suggesting that a large amount of defects were introduced into the samples during QSEM. The relative peak intensities of the processed samples are found to be comparable to the standard values of Cu in JCPDS cards (1990); therefore, there is no evident texture induced into the samples during QSEM. The XRD peak broadening FW(S) is related to the lattice strain ε_l through Williamson-Hall equation (Williamson and Hall, 1953) $\frac{FW(S)\cos\theta}{\lambda} = A_0 + 2\varepsilon_l\frac{\sin\theta}{\lambda}$, where λ and θ are X-ray wavelength and diffraction angle, respectively. A_0 is the coefficient of linear fit which is related to the size of the diffracting grains. Based on the experimental results in Fig. 6a, the relationship between FW(S)cosθ and sinθ is illustrated in Fig. 6b. It can be seen that, with the increasing shear strain in QSEM, the gradient of the regression line is increased, indicating that larger lattice strain was revealed. According to the linear fit in Fig. 6b, the lattice strain in processed copper can be obtained. Substituting the lattice strain ε_l into the equation (Williamson and Smallman, 1956) $\rho_T = 14.4\frac{\varepsilon_l^2}{b^2}$ where b is Burger's vector, the dislocation density ρ_T in processed copper is achieved. Fig. 7 shows the dislocation density measured by means of XRD. The dislocation density in the initial workpiece is $\sim 8 \times 10^{13}\,\mathrm{m}^{-2}$. The dislocation density in the processed copper is $\sim 10^{15}\ \mathrm{m}^{-2}$. The dislocation density increases with the increasing shear strain.

4. Theoretical analysis

4.1. Theoretical model

During QSEM, dislocation density ρ increases with plastic deformation ε. Referring to the model of Estrin and Mecking (1984), dislocation density ρ can be expressed as:

$$\frac{d\rho}{d\varepsilon} = \frac{1}{bd} + k_1\sqrt{\rho} - k_2\rho \tag{1}$$

In Eq. (1), ε is effective plastic strain, b is Burger's vector, d is the average grain size of initial workpiece, k_1 and k_2 are dislocation storage rate and dynamic recovery rate respectively.

The effective plastic strain ε increases from zero to $\gamma/\sqrt{3}$ during QSEM. The dislocation density ρ_0 for $\varepsilon = 0$ is the dislocation density of

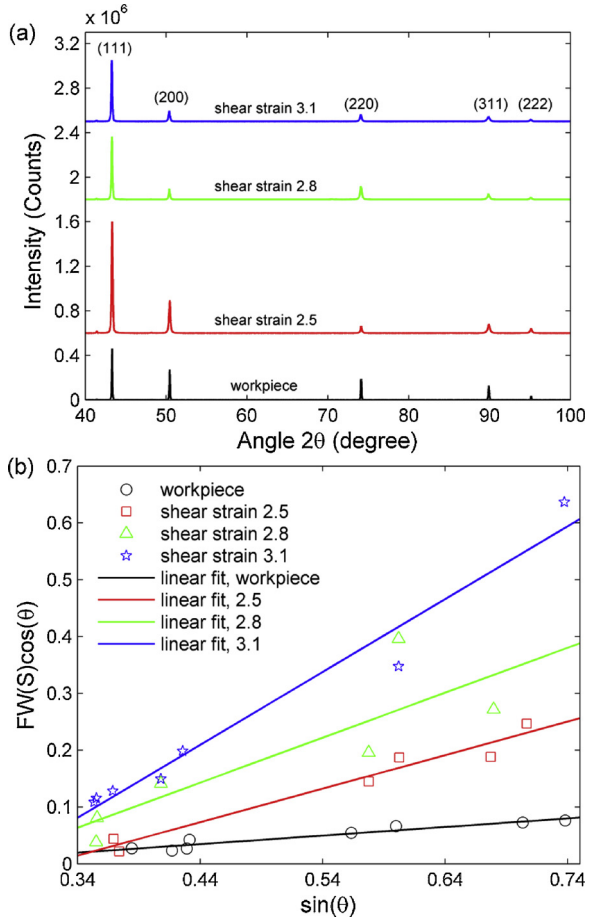

Fig. 6. (a) The X-ray diffraction (XRD) lines for different shear strains. (b) Relationship between FW(S)cosθ and sinθ for different shear strains, the gradient of the regression line provides the lattice strain.

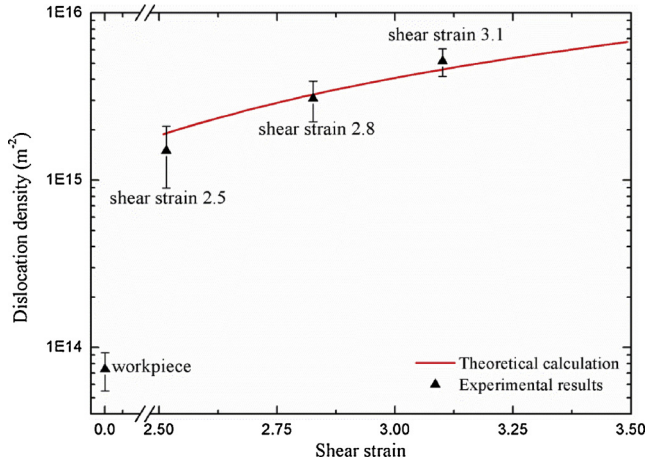

Fig. 7. Comparison of dislocation density between experimental results and theoretical calculations.

initial workpiece. Based on the experimental result in Fig. 7, the dislocation density ρ_0 in initial workpiece is $\sim 8 \times 10^{13} m^{-2}$. The dislocation density ρ_m after QSEM is obtained by solving Eq. (1) at the strain of $\gamma/\sqrt{3}$.

Copper sheets after QSEM were annealed at 523 K for 5 min, where recrystallization happens. According to the equation of Avrami (1939), recrystallization kinetics is given in the following form:

$$X = 1 - \exp(-Bt^n), \tag{2}$$

where X and t are volume fraction of recrystallization and annealing time respectively. B and n are affected by the type of recrystallization. If nucleation happens on grain boundary, n is equal to 2.

B is related to nucleation rate and nucleation growth rate:

$$B = I_0 \exp\left(-\frac{\Delta G}{k_B T}\right)\frac{2D_b\gamma_b V_m}{RT}\left(\frac{\rho_0}{\rho_m}\right)^2 \frac{1}{d_R}\left(\frac{1}{d^*} - \frac{1}{d_R}\right). \tag{3}$$

In Eq. (3), I_0 is reference nucleation rate, ΔG is critical nucleation energy, k_B is Boltzmann constant, D_b is boundary Self-diffusion coefficient, γ_b is boundary energy, V_m is molar volume, R is gas constant, and T is annealing temperature. d_R and d^* are recrystallized grain size and reference grain size respectively.

The volume fraction of remained SPD grains is $(1 - X)$ after heat treatment. The dislocation density ρ_h in SPDed grains after heat treatment is $\rho_h = (1 - X)\rho_m$. The microstructures after heat treatment are composed of SPDed grains and recrystallized grains. The yield strength σ_h after heat treatment is given by the rule-of-mixture equation:

$$\sigma_h = (1 - X)\beta G b\sqrt{\rho_h} + X\sigma_{rg}, \tag{4}$$

where G is shear modulus, β is a dislocation interaction term, and σ_{rg} is the yield strength of recrystallized grain.

According on Hall-Petch relationship derived by Hall (1951) and Petch (1953), the strength of recrystallized grain σ_{rg} is determined by the recrystallized grain size:

$$\sigma_{rg} = \sigma_0 + \frac{k}{\sqrt{d_R}}, \tag{5}$$

where σ_0 is a frictional stress required to move dislocation and k is the Hall-Petch slope.

The strain hardening rate H_h is obtained by taking the derivative of Eq. (4) with respect to strain:

$$H_h = (1 - X)\frac{\beta G b}{2\sqrt{\rho_h}}\left(\frac{1}{bd} + k_1\sqrt{\rho_h} - k_2\rho_h\right) + XH_{rg}, \tag{6}$$

where H_{rg} is the strain hardening rate of recrystallized grain.

4.2. Experimental validation

The material parameters for copper in Eqs. (1)–(6) can be directly referred from the relevant literatures. Others should be calculated by using the method and the data in the references for copper. The values of material parameters and the responding references are illustrated in Table 3. The evolution of dislocation density with the shear strain can be calculated by substituting the material parameters into the theoretical model of dislocation density ρ_h. It is shown in Fig.7 that the theoretical calculations are in agreement with the experimental results. The comparisons demonstrate that the theoretical model is valid to predict the dislocation density of the copper processed by QSEM and subsequent HT.

Substituting the parameters in Table 3 into Eqs. (1)–(6), the mechanical properties of copper after QSEM and subsequent HT can be calculated. Fig. 8 shows the variations of yield strength and strain hardening rate with shear strain. The yield strength of copper processed by the proposed strategy increases with the increasing shear strain (Fig. 8a); however, the strain hardening decreases with the increasing shear strain (Fig. 8b). The comparisons between theoretical results and experimental measurements are shown in Fig. 8. Both the yield strength and strain hardening rate predicted by the theoretical model are in accordance with the experimental measurements. Therefore, the theoretical model is valid to predict the mechanical properties of copper processed by QSEM and subsequent HT.

5. Discussion

Physical metallurgy has been widely used to process metallic

Table 3
Model parameters for copper.

Property	Value	Source
G	42.1 GPa	Literature from Frost and Ashby (1982)
b	0.256 nm	Idem
d	200 μm	Experiments in Fig. 4a
k_1	$8.5 \times 10^7 m^{-1}$	Literature from Ding and Guo (2001)
k_2	5.7×10^{-4}	Idem
β	0.5	Idem
D_b	$8\times 10^{-12} m^2/s$	Literature from Surholt and Herzig (1997)
γ_b	$0.5\, J/m^2$	Idem
R	8.314J/(mol·K)	Constant
V_m	$7.19 \times 10^{-6} m^3/mol$	Constant
k_B	$1.38 \times 10^{-23} J/K$	Constant
I_0	$3.45 \times 10^{14} m^{-1}s^{-1}$	Calculation based on literature of Avrami (1940)
ΔG	$1 \times 10^{-19} J$	Idem
d^*	4 μm	Experiments in Fig. 4b-d
d_R	5 μm	Experiments in Fig. 4b-d
σ_0	25.5 MPa	Literature from Meyers and Chawla (2009)
k	$0.11 MPa\sqrt{m}$	Idem
H_{rg}	1700 MPa	Calculation based on literature of Tian et al. (2018)

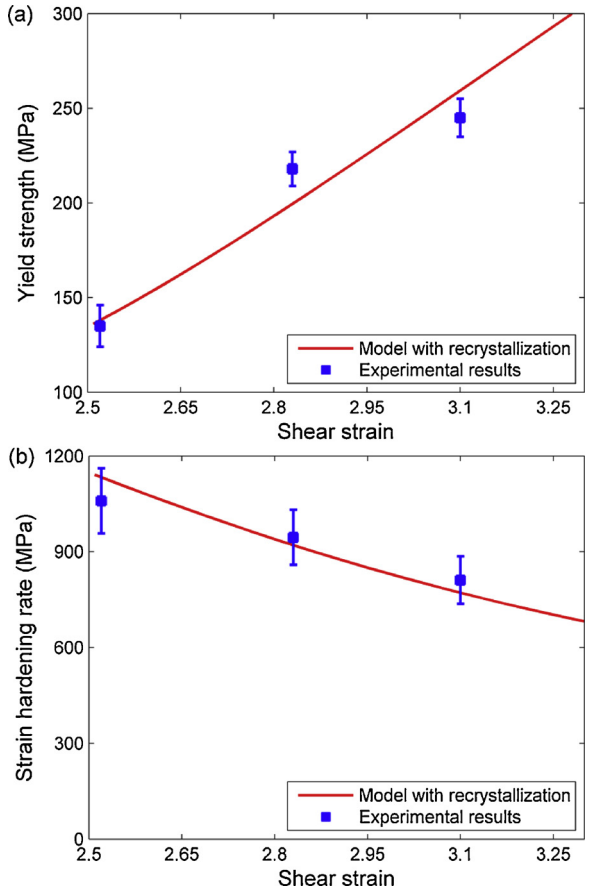

Fig. 8. Comparison of theoretical model and experimental results: (a) yield strength for different shear strain processed coppers; (b) strain hardening rate for different shear strain processed coppers.

materials for enhancing the mechanical properties. Heat treatment, as a type of physical metallurgy, is an effect method to improve the ductility of metallic materials. Annealing temperature and annealing time are two important parameters during heat treatment. As shown in the experiments of Yuan et al. (2015), with the increasing temperature, the strength decreases but the elongation increases. Nouroozi et al. (2018) found that both the work-hardening rate and final tensile properties

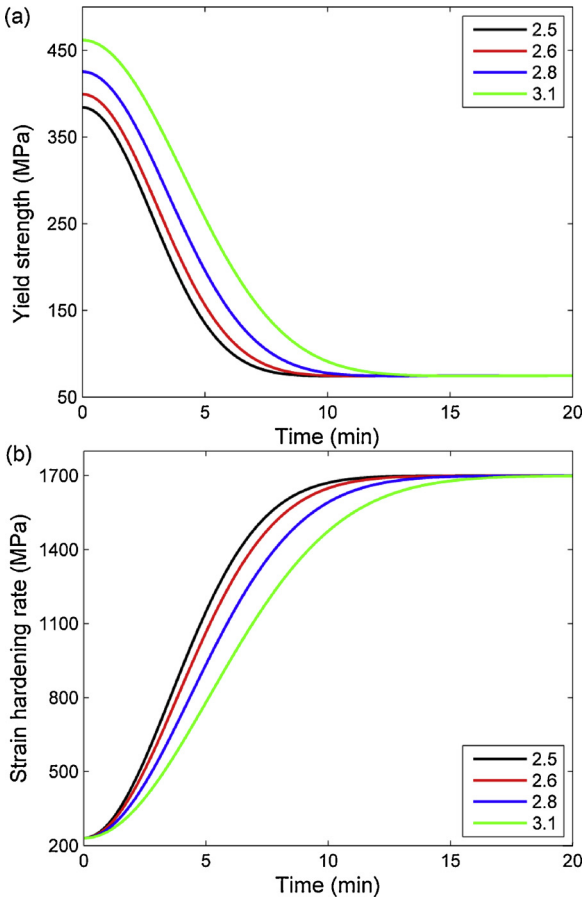

Fig. 9. (a) Variation of yield strength with annealing time at different shear strains; (b) Variation of strain hardening rate with annealing time at different shear strains.

decreases by increasing the annealing time beyond the optimum value. Therefore, the close controls of the annealing temperature and time are necessary for the enhancement of mechanical properties. In this section, the theoretical models are further used to discuss the influence of annealing time and annealing temperature on the mechanical properties of SPDed copper. The variations of mechanical properties with annealing time at different shear strains and annealing temperatures are shown in Figs. 9 and 10 respectively.

The variations of yield strength with annealing time at different processed shear strains are shown in Fig. 9a. For a given shear strain, yield strength decreases with the increasing annealing time, which is consistent with the trend in the experiments of Park et al. (2017). However, for a given annealing time, yield strength increases with the increasing shear strain. Fig. 9b shows the effect of annealing time and shear strain on the strain hardening rate. Strain hardening rate increases with the annealing time but decreases with the processed shear strain. When the annealing time is more than a certain value, the processed shear strain has no influence on the yield strength and strain hardening rate. If the annealing time is long enough, the mechanical properties of the processed coppers are the same as those of fully recrystallized grains (RGs).

The variations of yield strength with annealing time at different annealing temperatures are shown in Fig. 10a. For a given annealing temperature, yield strength decreases with the increasing annealing time. For a given annealing time, higher annealing temperature leads to lower yield strength, which is in accordance with the trend in the literature of Wang et al. (2018). Fig. 10b shows the effects of annealing time and annealing temperature on the strain hardening rate. Long annealing time or high annealing temperature could help to improve

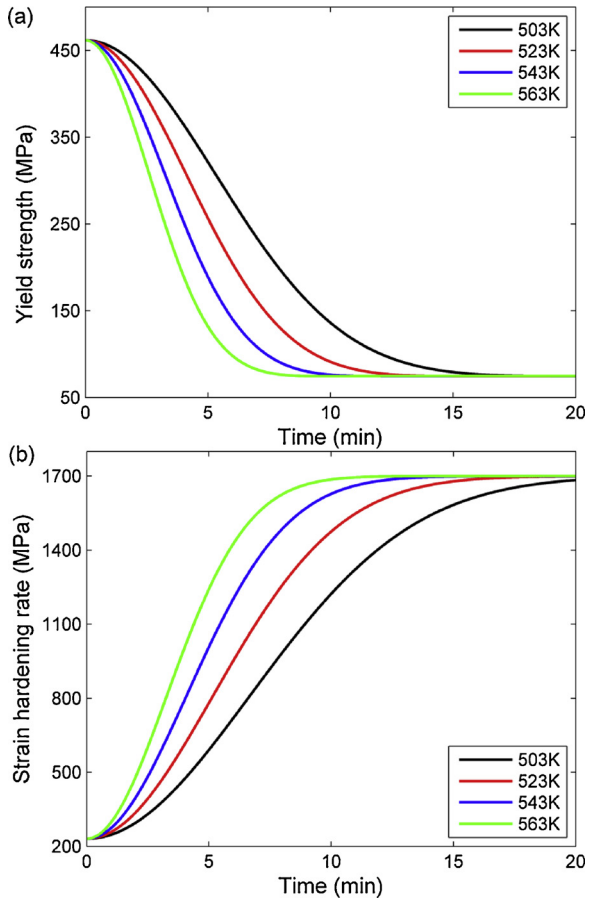

Fig. 10. (a) Variation of yield strength with annealing time at different annealing temperatures; (b) Variation of strain hardening rate with annealing time at different annealing temperatures.

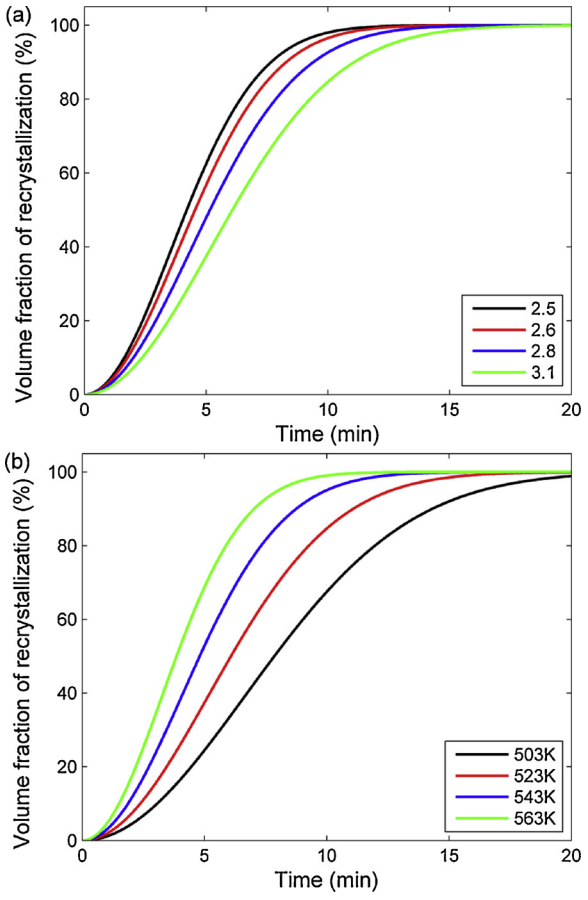

Fig. 11. Variation of volume fraction of recrystallization with annealing time: (a) at different shear strains; (b) at different annealing temperatures.

the strain hardening rate. When the processed copper is annealed at higher annealing temperature, less annealing time is needed to fabricate copper with the given mechanical properties.

Fig. 11 shows the variations of volume fraction of recrystallization with annealing time. The volume fraction of recrystallization increases with the increasing annealing time, which is in accordance with the trend in experiments of Park et al. (2017). Completed recrystallization happens if the annealing time is long enough. The volume fraction of recrystallization decreases with the increasing shear strain but increases with the increasing annealing temperature. With the increasing annealing time, the evolution trend of the volume fraction of recrystallization is in agreement with that of strain hardening rate. The formation of recrystallization leads to the decrease of forest dislocation produced in QSEM, inducing the low yield strength. Recrystallization helps to store the dislocation produced during tensile deformation, contributing to the improvement of strain hardening rate.

6. Concluding remarks

The mechanical properties of copper sheet, processed by combining severe plastic deformation (SPD) and heat treatment (HT), were investigated in this study. The following conclusions can be drawn.

(1) Quasi-static extrusion machining (QSEM) at the shear strain of 3.1 and subsequent heat treatment (HT) at 523 K for 5 min were used to enhance yield strength five times without compromising ductility in copper.
(2) Microstructural characterization shows that high strength and good ductility are attributed to the unique hierarchical microstructure: the recrystallized grains are surrounded by elongated subgrains with low angle grain boundaries (LAGBs).
(3) A theoretical model, considering dislocation storage, dislocation dynamic recovery and recrystallization, was employed to accurately predict the mechanical properties of the copper processed by QSEM and HT.

Acknowledgments

This work has been supported by the National Key Research and Development Program of China (No. 2017YFB0702003), the National Natural Science Foundation of China (Grant Nos. 11602236, 11132011 and 11802013), Fundamental Research Funds for the Central Universities (Grant No. FRF-BR-17-015A), the Strategic Priority Research Program of the Chinese Academy of Sciences (Grant Nos. XDB22040302, XDB22040303) and the Key Research Program of Frontier Sciences (Grant No. QYZDJSSW-JSC011).

Appendix A. Supplementary data

Supplementary material related to this article can be found, in the online version, at doi:https://doi.org/10.1016/j.jmatprotec.2018.12.001.

References

Avrami, M., 1939. Kinetics of phase change. I. J. Chem. Phys. 7, 1103–1112.
Avrami, M., 1940. Kinetics of phase change. II Transformation time relations for random distribution of nuclei. J. Chem. Phys. 8, 212–221.
Brown, T.L., Saldana, C., Murthy, T.G., Mann, J.B., Guo, Y., Allard, L.F., King, A.H., Compton, W.D., Trumble, K.P., Chandrasekar, S., 2009. A study of the interactive

effects of strain, strain rate and temperature in LSEM of copper. Acta Mater. 57, 5491–5500.
Cai, S.L., Chen, Y., Ye, G.G., Jiang, M.Q., Wang, H.Y., Dai, L.H., 2015. Characterization of the deformation field in large-strain extrusion machining. J. Mater. Process. Technol. 216, 48–58.
Ceretti, E., Lucchi, M., Altan, T., 1999. FEM simulation of orthogonal cutting: serrated chip formation. J. Mater. Process. Technol. 95, 17–26.
Childs, T.H.C., 2013. Ductile shear failure damage modelling and predicting built-up edge in steel machining. J. Mater. Process. Technol. 213, 1954–1969.
Christian, J.W., Mahajan, S., 1995. Deformation twinning. Prog. Mater. Sci. 39, 1–157.
Cox, D.E., Hastings, J.B., Cardoso, L.P., Finger, L.W., 1986. Synchrotron X-Ray powder diffraction at X13A: a dedicated powder diffractometer at the national synchrotron light source. Mater. Sci. Forum 9, 1–20.
Ding, R., Guo, Z.X., 2001. Coupled quantitative simulation of microstructural evolution and plastic flow during dynamic recrystallization. Acta Mater. 49, 3163–3175.
Dolata-Grosz, A., Śleziona, J., Formanek, B., 2006. Structure and properties of aluminium cast composites strengthened by dispersion phases. J. Mater. Process. Technol. 175, 192–197.
Estrin, Y., Mecking, H., 1984. A unified phenomenological description of work hardening and creep based on one-parameter models. Acta Metall. 32, 57–70.
Fang, H., Li, W.L., Tao, N.R., Lu, K., 2011. Revealing extraordinary intrinsic tensile plasticity in gradient nano-grained copper. Science 331, 1587–1590.
Frost, H.J., Ashby, M.F., 1982. Deformation-Mechanism Maps: the plasticity and creep of metals and ceramics Pergamon Press. Oxford.
Güzel, A., Jäger, A., Parvizian, F., Lambers, H.G., Tekkaya, A.E., Svendsen, B., Maier, H.J., 2012. A new method for determining dynamic grain structure evolution during hot aluminum extrusion. J. Mater. Process. Technol. 212, 323–330.
Hall, E.O., 1951. The deformation and ageing of mild steel: III discussion of results. Proc. Phys. Soc. B 64, 747–753.
Huo, W.T., Shi, J.T., Hou, L.G., Zhang, J.S., 2017. An improved thermo-mechanical treatment of high-strength Al–Zn–Mg–Cu alloy for effective grain refinement and ductility modification. J. Mater. Process. Technol. 239, 303–314.
Jia, D., Wang, Y.M., Ramesh, K.T., Ma, E., Zhu, Y.T., Valiev, R.Z., 2001. Deformation behavior and plastic instabilities of ultrafine-grained titanium. Appl. Phys. Lett. 79, 611–613.
Jiang, R., Everitt, S., Lewandowski, M., Gao, N., Reed, P.A.S., 2014. Grain size effects in a Ni-based turbine disc alloy in the time and cycle dependent crack growth regimes. Int. J. Fatigue 62, 217–227.
Kauffmann, A., Freudenberger, J., Klauß, H., Klemm, V., Schillinger, W., Subramanya Sarma, V., Schultz, L., 2013. Properties of cryo-drawn copper with severely twinned microstructure. Mater. Sci. Eng. A 588, 132–141.
Liu, X., Wu, K., Wu, G., Gao, Y., Zhu, L., Lu, Y., Lu, J., 2016a. High strength and high ductility copper obtained by topologically controlled planar heterogeneous structures. Scr. Mater. 124, 103–107.
Liu, Y., Cai, S., Dai, L., 2016b. A new method for grain refinement in magnesium alloy: high speed extrusion machining. Mater. Sci. Eng. A 651, 878–885.
Lobos, J., Suzuki, S., Utsunomiya, H., Nakajima, H., Rodrigez-Perez, M.A., 2010. Strengthening of lotus-type porous copper by ECAE process. J. Mater. Process. Technol. 212, 2007–2011.
Lu, L., Shen, Y.F., Chen, X.H., Qian, L.H., Lu, K., 2004. Ultrahigh strength and high electrical conductivity in copper. Science 304, 422–426.
Lu, K., Lu, L., Suresh, S., 2009. Strengthening materials by engineering coherent internal boundaries at the nanoscale. Science 324, 349.
Meyers, M.A., Chawla, K.K., 2009. Mechanical Behavior of Materials (Second Edition). Cambridge University Press, Cambridge.
Meyers, M.A., Mishra, A., Benson, D.J., 2006. Mechanical properties of nanocrystalline materials. Prog. Mater. Sci. 51, 427–556.
Moscoso, W., Shankar, M.R., Mann, J.B., Compton, W., Chandrasekar, S., 2007. Bulk nanostructure materials by LSEM. J. Mater. Res. 22, 201–205.
Nag, S., Sardar, P., Jain, A., Himanshu, A., Mondal, D.K., 2014. Correlation between ferrite grain size, microstructure and tensile properties of 0.17 wt% carbon steel with traces of microalloying elements. Mater. Sci. Eng. A 597, 253–263.
Nouroozi, M., Mirzadeh, H., Zamani, M., 2018. Effect of microstructural refinement and intercritical annealing time on mechanical properties of high-formability dual phase steel. Mater. Sci. Eng. A 736, 22–26.
Park, J.-W., Jeong, H.-J., Jin, S.-W., Kim, M.-J., Lee, K., Kim, J.J., Hong, S.-T., Han, H.N., 2017. Effect of electric current on recrystallization kinetics in interstitial free steel and AZ31 magnesium alloy. Mater. Charact. 133, 70–76.
Petch, N.J., 1953. The cleavage strength of polycrystals. J. Iron Steel Inst. 174, 25–28.
Petryk, H., Stupkiewicz, S., Kuziak, R., 2008. Grain refinement and strain hardening in IF steel during multi-axis compression: experiment and modelling. J. Mater. Process. Technol. 204, 255–263.
Powder Diffraction File, 1990. Joint Committee on Powder Diffraction Standards. Swarthmore, PA. .
Richert, M., Liu, Q., Hansen, N., 1999. Microstructural evolution over a large strain range in aluminium deformed by cyclic-extrusion–compression. Mater. Sci. Eng. A 260, 275–283.
Saito, Y., Utsunomiya, H., Tsuji, N., Sakai, T., 1999. Novel ultra-high straining process for bulk materials—development of the accumulative roll-bonding (ARB) process. Acta Mater. 47, 579–583.
Segal, V.M., Reznikov, V.I., Drobyshevskiy, A.E., Kopylov, V.I., 1981. Plastic working of metals by simple shear. Russ. Metall. 1, 99–105.
Smirnova, N.A., Levit, V.I., Pilyugin, V.I., Kuznetsov, R.I., Davydova, L.S., Sazonova, V.A., 1986. Evolution of the fcc single-crystal structure during severe plastic deformations. Fizika Metallov I Metallovedenie 61, 1170–1177.
Su, J.-h., Liu, P., Dong, Q.-m., Li, H.-j., Ren, F.-z., 2008. Aging study of rapidly solidified and solid-solution Cu–Cr–Sn–Zn alloy. J. Mater. Process. Technol. 205, 366–369.
Surholt, T., Herzig, C., 1997. Grain boundary self- and solute diffusion and segregation in general large angle grain boundaries in copper. Defect Diffus. Forum 143-147, 1391–1396.
Tian, Y.Z., Gao, S., Zhao, L.J., Lu, S., Pippan, R., Zhang, Z.F., Tsuji, N., 2018. Remarkable transitions of yield behavior and Lüders deformation in pure Cu by changing grain sizes. Scr. Mater. 142, 88–91.
Umbrello, D., Rizzuti, S., Outeiro, J.C., Shivpuri, R., M'Saoubi, R., 2008. Hardness-based flow stress for numerical simulation of hard machining AISI H13 tool steel. J. Mater. Process. Technol. 199, 64–73.
Valiev, R.Z., Islamgaliev, R.K., Alexandrov, I.V., 2000. Bulk nanostructured materials from severe plastic deformation. Prog. Mater. Sci. 45, 103–189.
Wang, Y., Chen, M., Zhou, F., Ma, E., 2002. High tensile ductility in a nanostructured metal. Nature 419, 912–915.
Wang, Z., Bei, H., Baker, I., 2018. Microband induced plasticity and the temperature dependence of the mechanical properties of a carbon-doped FeNiMnAlCr high entropy alloy. Mater. Charact. 139, 373–381.
Williamson, G.K., Hall, W.H., 1953. X-ray line broadening from filed aluminium and wolfram. Acta Metall. 1, 22–31.
Williamson, G.K., Smallman, R.E., 1956. III. Dislocation densities in some annealed and cold-worked metals from measurements on the X-ray debye-scherrer spectrum. Philos. Mag. 1, 34–46.
Wu, X.L., Jiang, P., Chen, L., Yuan, F.P., Zhu, Y.T., 2014. Extraordinary strain hardening by gradient structure. Proc. Natl. Acad. Sci. 111, 7197–7201.
Yuan, X., Chen, L., Zhao, Y., Di, H., Zhu, F., 2015. Influence of annealing temperature on mechanical properties and microstructures of a high manganese austenitic steel. J. Mater. Process. Technol. 217, 278–285.
Zhu, Y.T., Liao, X.Z., 2004. Nanostructured matels: retaining ductility. Nat. Mater. 3, 351–352.